

# Paleoceanography and Paleoclimatology

## RESEARCH ARTICLE

10.1029/2019PA003793

### Key Points:

- As the AMOC weakens, Nordic Sea sea ice and convection sites shift equatorward and the Deep Western Boundary Current weakens proportionally
- As the AMOC weakens, the southward flow on the eastern side of the Mid-Atlantic Ridge strengthens by up to 100%
- Proxy records are consistent with both weaker NADW and AABW at the Last Glacial Maximum

### Supporting Information:

- Supporting Information S1

### Correspondence to:

L. Menviel,  
l.menviel@unsw.edu.au

### Citation:

Menviel, L. C., Spence, P., Skinner, L. C., Tachikawa, K., Friedrich, T., Missiaen, L., & Yu, J. (2020). Enhanced middepth southward transport in the northeast Atlantic at the Last Glacial Maximum despite a weaker AMOC. *Paleoceanography and Paleoclimatology*, 35, e2019PA003793. <https://doi.org/10.1029/2019PA003793>

Received 13 OCT 2019

Accepted 17 JAN 2020

Accepted article online 3 FEB 2020

## Enhanced Mid-depth Southward Transport in the Northeast Atlantic at the Last Glacial Maximum Despite a Weaker AMOC

L. C. Menviel<sup>1,2</sup>, P. Spence<sup>1</sup>, L. C. Skinner<sup>3</sup>, K. Tachikawa<sup>4</sup>, T. Friedrich<sup>5</sup>, L. Missiaen<sup>1</sup>, and J. Yu<sup>6</sup>

<sup>1</sup>Climate Change Research Centre, University of New South Wales, Sydney, New South Wales, Australia, <sup>2</sup>PANGAEA, University of New South Wales, Sydney, New South Wales, Australia, <sup>3</sup>Department of Earth Sciences, University of Cambridge, Cambridge, UK, <sup>4</sup>Aix Marseille Univ., CNRS, IRD, Coll France, CEREGE, Aix-en-Provence, France, <sup>5</sup>Department of Oceanography, University of Hawai'i at Mānoa, Honolulu, HI, USA, <sup>6</sup>Research School of Earth Sciences, Australian National University, Canberra, ACT, Australia

**Abstract** While previous studies consistently suggest that North Atlantic Deep Water (NADW) was shallower at the Last Glacial Maximum (LGM) than at pre-industrial, its strength is still controversial. Here, using a series of LGM experiments, we show that proxy records are consistent with a shallower and ~50% weaker NADW, associated with a ~3° equatorward shift of the sea ice edge and convection sites in the Norwegian Sea. A shoaling and weakening of NADW further allow penetration of Antarctic Bottom Water in the North Atlantic, despite Antarctic Bottom Water transport being reduced by ~40%. While the Deep Western Boundary Current in the northwest Atlantic weakens with NADW, the mid-depth southward flow on the east side of the north Mid-Atlantic Ridge strengthens, consistent with paleorecords. This northeast Atlantic intensification is due to a change in density gradients: a weaker AMOC reduces the transport of equatorial waters to the northeast Atlantic, thus weakening the North Atlantic zonal density gradient. The resultant globally weaker oceanic circulation at the LGM would have contributed to an increase in oceanic carbon content and thus a decrease in atmospheric CO<sub>2</sub> concentration.

## 1. Introduction

The Atlantic Meridional Overturning Circulation (AMOC), which is defined by the zonally integrated flow in the Atlantic, depends on North Atlantic Deep Water (NADW) and Antarctic Bottom Water (AABW) transport in the Atlantic basin. Today, NADW is composed of Labrador Sea Water (LSW), Denmark Strait Overflow Water, and Iceland-Scotland Overflow Water, which are formed by deep ocean convection and brine rejection in the Labrador Sea and Nordic Seas, respectively (Bullister et al., 2013). In the subpolar North Atlantic, these water masses merge and flow southward along the Deep Western Boundary Current (Talley et al., 2011). The surface and subsurface circulation of the North Atlantic are also influenced by the AMOC, with one of the main features of the upper branch of the AMOC being the Gulf Stream and its extension the North Atlantic Current (NAC). The Gulf Stream follows the east coast of North America from the tip of Florida to Newfoundland, after which it crosses the Atlantic as the NAC bringing warm waters to the northeast Atlantic. Despite the AMOC influence on climate and on the global carbon cycle, past changes in its strength are still a matter of debate, and in particular its state at the Last Glacial Maximum (LGM, ~21,000 years ago) (e.g., Hesse et al., 2011; Kurahashi-Nakamura et al., 2017; Lippold et al., 2012; Menviel et al., 2017).

The LGM was characterized by a global mean sea level ~134 m lower than present (Lambeck et al., 2014) due to large continental ice sheets covering North America and Eurasia (e.g., Abe-Ouchi et al., 2015; Tarasov et al., 2012) and by a concentration of atmospheric carbon dioxide (CO<sub>2</sub>) ~100 ppm lower (Marcott et al., 2011). At the LGM, NADW formation was most likely different from today due to the significant sea ice advance in the Labrador and Nordic Seas (Yang et al., 2006).

The different geochemical properties of NADW and AABW have been used to reconstruct their extent in the Atlantic at the LGM. NADW is characterized by low nutrients (e.g., PO<sub>4</sub>) and dissolved inorganic carbon (DIC) concentrations, as well as high carbonate ions content, because most surface nutrients are utilized

by phytoplankton within the NAC. Since carbon isotope fractionation mostly occurs during photosynthesis, preferentially incorporating  $^{12}\text{C}$  into organic matter, NADW has relatively high  $\delta^{13}\text{C}$  values. In contrast, due to low nutrient utilization at the surface of the Southern Ocean, AABW displays a high nutrient content and low  $\delta^{13}\text{C}$  values. Neodymium (Nd) isotopic ratios ( $^{143}\text{Nd}/^{144}\text{Nd}$ ,  $\epsilon\text{Nd}$ ) have also been used to infer changes in the Atlantic ocean circulation as the NADW end-member has a much lower  $\epsilon\text{Nd}$  ( $\sim -12.3 \pm 0.9$ ) than AABW ( $\sim -8.6 \pm 0.6$ ) (Tachikawa et al., 2017). Lower  $\text{PO}_4$  (Marchitto, 2006), and higher carbonate ions content (Yu et al., 2008), as well as higher benthic  $\delta^{13}\text{C}$  (Curry & Oppo, 2005) and  $\epsilon\text{Nd}$  (Howe et al., 2016) in the upper 2,000 m of the North Atlantic at the LGM have thus been interpreted as indicating a shallower NADW. An expansion of AABW into the deep North Atlantic has been deduced from higher  $\text{PO}_4$  content, lower  $\delta^{13}\text{C}$  values below 2,500 m depth (Curry & Oppo, 2005; Marchitto, 2006), and higher  $\epsilon\text{Nd}$  (Howe et al., 2016).

However, assessing the AMOC strength at the LGM has proven more elusive and controversial because no proxies can provide a quantitative estimate of the AMOC strength. Radiocarbon “ventilation ages” inform on the rate of ventilation but are complicated by the impacts of variable air-sea gas exchange efficiency and water mass sourcing (e.g., Skinner et al., 2017). Since  $^{231}\text{Pa}$  has a much longer residence time than  $^{230}\text{Th}$  in the ocean, sedimentary  $^{231}\text{Pa}/^{230}\text{Th}$  has also been used as a proxy for AMOC strength (e.g., Henry et al., 2016; McManus et al., 2004). Higher ventilation ages below 2,000 m depth in the North Atlantic (Freeman et al., 2016; Skinner et al., 2017) as well as changes in vertical  $^{231}\text{Pa}/^{230}\text{Th}$  profiles (Bradtmeier et al., 2014; Gherardi et al., 2005; Lippold et al., 2012, 2016; McManus et al., 2004; Ng et al., 2018) support a shoaling of NADW and enhanced AABW incursion. However, while  $^{231}\text{Pa}/^{230}\text{Th}$  (Gherardi et al., 2005; Lippold et al., 2016; McManus et al., 2004; Ng et al., 2018) records from the northwest Atlantic suggest a weaker LGM NADW transport, records from the northeast Atlantic suggest that the LGM mid-depth (here defined as  $\sim 1,500$  to 3,000 m depth) transport was as strong as during pre-industrial (PI) (Balmer & Sarnthein, 2018; Gherardi et al., 2005; Lippold et al., 2012), despite some radiocarbon evidence for poor ventilation below 2,000 m depth (Freeman et al., 2016; Skinner et al., 2017).

The latest LGM simulations performed as part of the Paleoclimate Modelling Intercomparison Project phase 3 (PMIP3) cannot inform on the possible AMOC strength at the LGM, as all models, apart from CCSM4, simulate a deeper boundary between NADW and AABW (Muglia & Schmittner, 2015), in contrast to what is suggested by paleo-records. The consistent AMOC strengthening and deepening in these PMIP3 LGM simulations has been partly attributed to stronger North Atlantic windstress (Muglia & Schmittner, 2015). Only CCSM4 displays a 275 m shoaling of NADW with a marginal strengthening of 1.8 Sv (+9%), but it has not been shown whether this small AMOC change would lead to a tracer distribution that would be in agreement with paleoproxy records.

To further our understanding of the LGM AMOC, the sensitivity of nutrients,  $\delta^{18}\text{O}$ ,  $\delta^{13}\text{C}$ , or ventilation ages to different Atlantic oceanic circulation states has been tested and compared to paleorecords (e.g., Hesse et al., 2011; Kurahashi-Nakamura et al., 2017; Menviel et al., 2017; Muglia et al., 2018; Tagliabue et al., 2009). These model outputs/paleodata comparisons provide additional evidence for a shoaling of NADW at the LGM but do not provide a consensus on the change in AMOC strength. However, to date, no modeling study has looked into how AMOC changes at the LGM could impact the mid-depth oceanic circulation and particularly zonal differences across the North Atlantic.

Here, using a suite of experiments performed with an Earth system model, which includes  $\delta^{13}\text{C}$ , radiocarbon, and  $\epsilon\text{Nd}$ , we study the relations between location of deep ocean convection in the Nordic and Labrador Seas, NADW and AABW transport, and the strength of North Atlantic mid-depth ocean currents. The resulting North Atlantic tracer profiles are compared to existing paleoproxy records, in order to assess whether the zonal differences recorded in North Atlantic proxy records can be explained, and whether this can inform on the LGM AMOC strength.

## 2. Methods

A series of LGM experiments is performed with the Earth system model of intermediate complexity LOVECLIM. LOVECLIM includes an ocean general circulation model ( $3^\circ$  by  $3^\circ$ , 20 vertical levels), fully coupled to a dynamic-thermodynamic sea ice model, a quasi-geostrophic atmospheric model (T21 resolution), and a land and marine carbon cycle model (Goosse et al., 2010). The model also includes carbon isotopes (Menviel et al., 2015) and  $\epsilon\text{Nd}$  (Friedrich et al., 2014).

A set of LGM experiments with different oceanic circulation states performed with the carbon isotopes-enabled version of LOVECLIM is described in Menviel et al. (2017). However, since these experiments did not include  $\epsilon\text{Nd}$ , a new series of LGM experiments is performed. The initial conditions of the experiments are taken from a LGM experiment (*V3L* in Menviel et al., 2017), which features a strong AMOC, and a mean LGM oceanic  $\delta^{13}\text{C}$  that is  $\sim 0.34\text{‰}$  lower than at PI. From there, LOVECLIM is equilibrated to LGM boundary conditions by applying appropriate orbital parameters (Berger, 1978), Northern Hemisphere ice sheets topography and albedo (Abe-Ouchi et al., 2007), atmospheric greenhouse gases concentrations (190 ppm for  $\text{CO}_2$ , 379.12 ppb for  $\text{CH}_4$  and 199 ppb for  $\text{N}_2\text{O}$ ), and their isotopic values ( $-6.45\text{‰}$  for  $\delta^{13}\text{CO}_2$  and  $400\text{‰}$  for  $\Delta^{14}\text{CO}_2$ ), as well as a closed Bering Strait.

The default LGM experiment thus obtained displays a strong AMOC and is referred to as *LNAs*. To mimic the background meltwater runoff from the large Northern Hemisphere ice sheets, which is not captured by our model setup, freshwater is added (0.1 Sv) into the North Atlantic for 3,000 years (*LNaw*). The model setup does not take into account the advance of the glacial Antarctic ice sheet onto the Ross and Weddell Seas (Bentley et al., 2014), which are the main regions of AABW formation today. Ice sheet advance onto the Antarctic continental shelves could have led to a weaker AABW formation at the LGM than PI. Starting from *LNaw*, AABW is weakened by adding meltwater into the Southern Ocean (0.07 Sv, *LNaw-SOW*). Finally, it has been hypothesized that the strength of the Southern Ocean upwelling, mainly modulated by the Southern Hemispheric westerlies, would provide a strong control on carbon transfer from the deep ocean to the atmosphere, and thus on the atmospheric  $\text{CO}_2$  concentration (Toggweiler et al., 2006). To account for potential changes in the strength of the Southern Hemispheric westerlies, that might not be captured by LOVECLIM, additional simulations are forced by a 20% weakening of the Southern Hemispheric westerlies (*LNaw-SHWw*), or both a Southern Ocean meltwater input and a weakening of the Southern Hemispheric westerlies (*LNaw-SOW-SHWw*).

As there are some small differences in initial conditions and forcings applied across the LGM experiments described in Menviel et al. (2017) and the ones performed here, the resultant oceanic circulation states differ slightly (supporting information Table S1). Therefore, both set of experiments are included here, as this provides a larger ensemble of simulations to study the relationship between AMOC strength and currents with greater statistical confidence.

To understand the processes leading to changes in North Atlantic  $\delta^{13}\text{C}$  between the LGM and PI,  $\delta^{13}\text{C}$  anomalies ( $\Delta\delta^{13}\text{C}$ ) are decomposed into their biological ( $\delta^{13}\text{C}_{\text{BIO}}$ ) and thermodynamic ( $\delta^{13}\text{C}_{\text{TH}}$ ) components. Since there is no fractionation during carbonate precipitation in this version of the model, the biological impact on  $\delta^{13}\text{C}$  can be estimated by the change in remineralized carbon ( $C_{\text{org}}$ ):

$$\delta^{13}\text{C}_{\text{BIO}} = \frac{\delta^{13}\text{C}_{\text{org}} * 12}{12\text{C}} = \frac{\delta^{13}\text{C}_{\text{org}} * R_{\text{c/p}} * P_{\text{Rem}}}{12\text{C}} \quad (1)$$

with  $-20\text{‰}$  for  $\delta^{13}\text{C}_{\text{org}}$ ,  $P_{\text{Rem}}$  phosphate generated through remineralization and estimated from the apparent oxygen utilization (AOU) ( $P_{\text{Rem}} = \text{AOU}/R_{\text{o/p}}$ ).  $R_{\text{c/p}}$  and  $R_{\text{o/p}}$  are the carbon over phosphate and oxygen over phosphate Redfield ratios equal to 117 and 170, respectively.  $\Delta\delta^{13}\text{C}_{\text{TH}}$  reflects the changes in  $\delta^{13}\text{C}$  due to air-sea gas exchange and temperature and is estimated by  $\Delta\delta^{13}\text{C}_{\text{TH}} = \Delta\delta^{13}\text{C} - \Delta\delta^{13}\text{C}_{\text{BIO}}$ .

This decomposition assumes that dissolved oxygen in the ocean could have reached equilibrium everywhere. Due to disequilibrium during air-sea gas exchange, AOU changes might be overestimated and therefore so might be  $\delta^{13}\text{C}_{\text{BIO}}$  estimates (Khatriwala et al., 2019).

### 3. Sea Ice and Deep Ocean Convection

The preindustrial (*PI*) experiment is characterized by a strong AMOC ( $\sim 25$  Sv, Figure 1a), with deep ocean convection occurring in the Norwegian Sea, the Labrador Sea, and south of Iceland (Figure 2a). In agreement with recent data from the Overturning in the Subpolar North Atlantic Program (Lozier et al., 2019), the transport between Greenland and Scotland dominates the overturning and varies between  $\sim 10$  and 17 Sv.

Under LGM conditions, the model simulates an AMOC as strong as *PI* ( $\sim 25$  Sv, Figure 1b, *LNAs*), but with NADW reaching the abyssal North Atlantic and filling most of the Atlantic basin. Several processes lead to this strong LGM AMOC: colder conditions, the closure of the Bering Strait (Hu et al., 2012), and stronger polar easterlies in the Nordic Seas. Deep ocean convection still occurs in the Norwegian Sea and south of

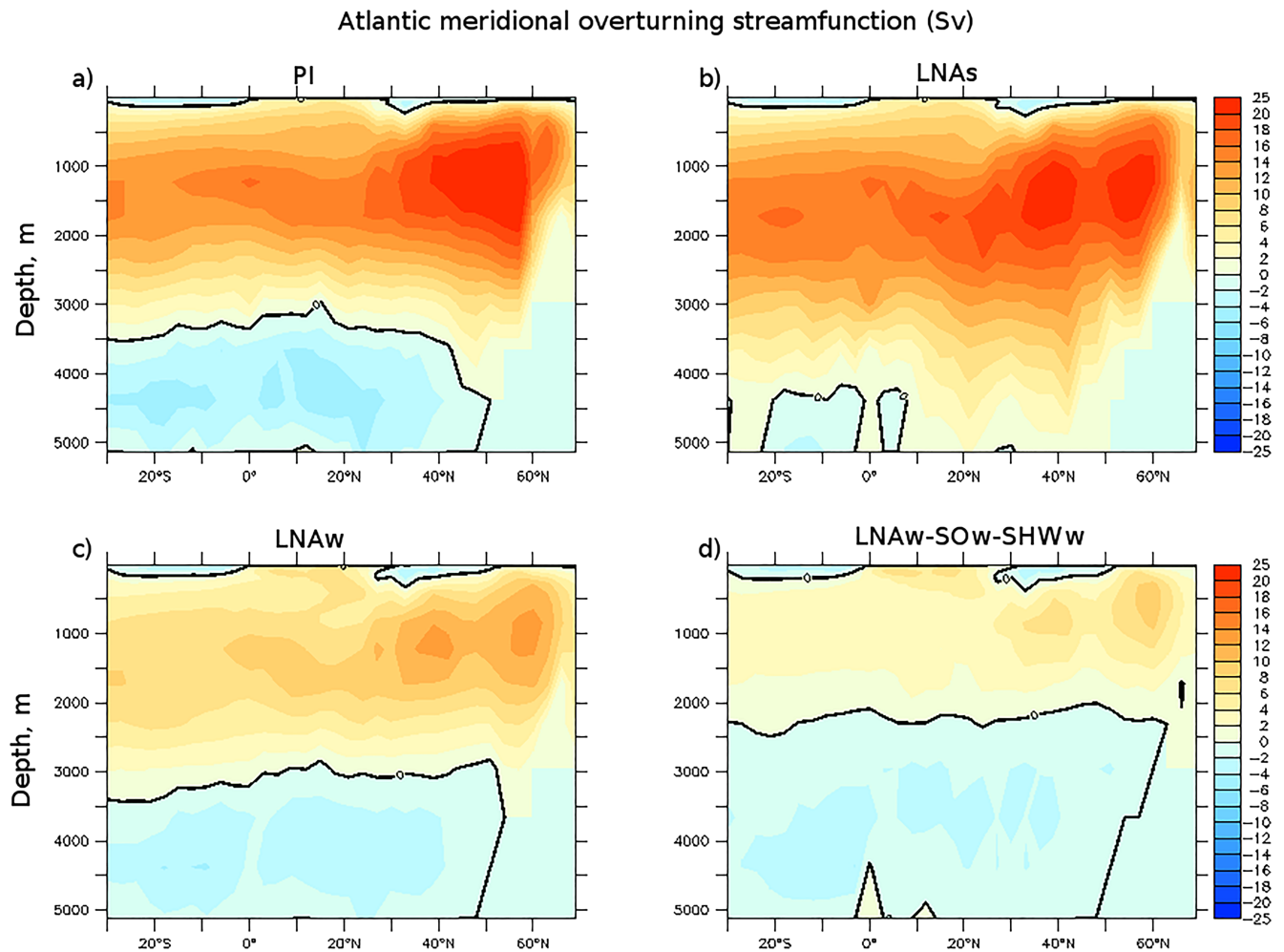


**Figure 1.** Meridional overturning streamfunction in the Atlantic basin (Sv) for (a) the preindustrial control run (*PI*), the LGM state with (b) strong NADW (*LNAs*), (c) weak NADW (*LNAw*), and (d) weak NADW and weak AABW (*LNAw-SOw-SHWw*). The 0 Sv line is in black.

Iceland (Figure 2b), but sea ice advance over the Labrador Sea inhibits deep ocean convection in that region. In fact, all the simulations performed here suggest that there is no LSW under LGM conditions due to the sea ice advance. As LSW has a very low  $\epsilon Nd$ , a lack of LSW induces positive  $\epsilon Nd$  anomalies in the deep northwest Atlantic (Figure 3i), in agreement with LGM  $\epsilon Nd$  values from the western Atlantic (Böhm et al., 2015; Howe et al., 2016; Lippold et al., 2016).

However, paleoproxy records do not support strong NADW transport below 3,000 m depth at the LGM, and some processes, such as increased runoff from surrounding ice sheets, are not included in the model. When meltwater is added to the North Atlantic, the AMOC weakens to 14.7 Sv (Figure 1c, *LNAw*). Greater stratification and a reduced meridional heat transport to the North Atlantic due to weaker AMOC (Krebs & Timmermann, 2007) induces a 3° equatorward shift of the winter sea ice edge in the Norwegian Sea (Figure 2c). The lack of deep-ocean convection during boreal summer leads to an advance of the summer sea ice edge in the Nordic Seas to ~ 65°N and to 55°N on the western side of the Labrador Sea.

The AABW, defined here as the minimum of the meridional overturning streamfunction in the Southern Ocean, is strong at -12.6 Sv for *PI*, and -14.6 Sv for both *LNAs* and *LNAw*. Despite AABW being strong in *LNAs*, it does not penetrate into the North Atlantic because the strong and deep NADW prevents it. A modification of both the buoyancy and dynamic forcing over the Southern Ocean causes a reduction of AABW formation to -7.8 Sv, but also reduces the Southern Ocean upwelling, which in turns weakens the AMOC to 11.2 Sv (Figure 1d, *LNAw-SOw-SHWw*, Methods). This AMOC weakening further cools the northeast Atlantic, shifting both the winter and summer sea ice edges by an additional ~ 2° southward, and restricting deep ocean convection to a small area in the southern part of the Norwegian Sea, as well as south of



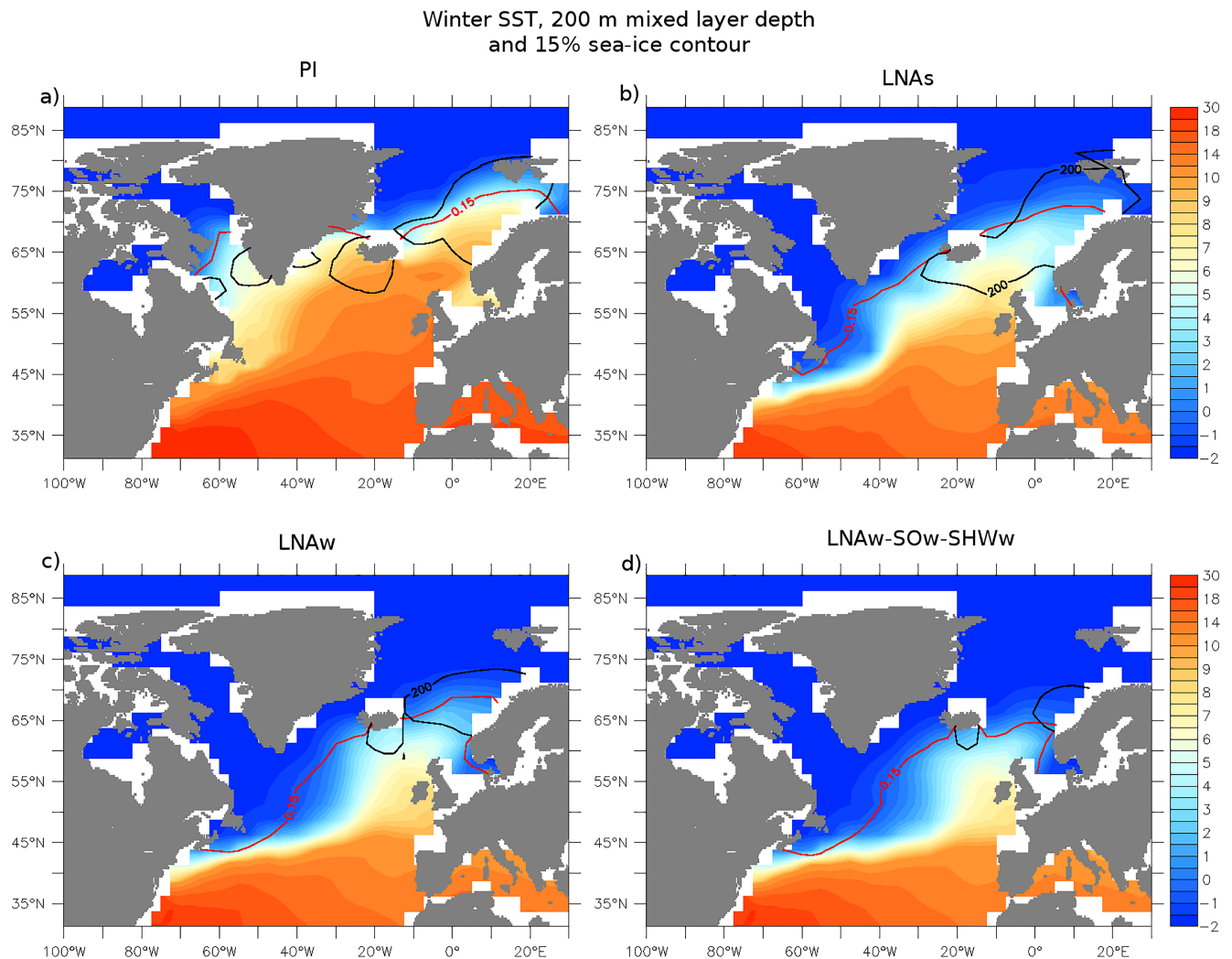


**Figure 2.** Winter SST (shading, °C), mixed layer depth (black contour, 200 m) and 15% sea ice concentration (red contour) for (a) the preindustrial experiment, and the LGM states with (b) a strong NADW (*LNAs*), (c) a weak NADW (*LNAw*), and (d) weak NADW and weak AABW (*LNAw-SOw-SHWw*).

Iceland (Figure 2d). The AMOC weakening is also associated with a significant shoaling of the NADW/AABW boundary to 2,400 m depth, further away from bottom topography, which reduces mixing and increases stratification (De Boer & Hogg, 2014), as seen in the North Atlantic vertical tracer distribution (Figure 3).

#### 4. North Atlantic Middepth Currents

At PI, the Deep Western Boundary Current (DWBC), a southward flow occurring between 1,500 and 3,500 m depth in the northwest Atlantic, is strong (Figures 4a and 5a, black circle, ~15 Sv) and overlays an abyssal northern flow of southern-sourced waters. Under LGM conditions, when NADW is strong, the DWBC transport is similar but deeper, with the southward flow dominating below ~2,000 m depth (Figures 4b and 5a, blue triangle). As the AMOC weakens, so does the DWBC ( $R = 0.95$ , Figure 5a), which also shoals, thus allowing an abyssal northern flow of southern-sourced waters (Figures 4c and 4d). Despite its weaker global transport in experiment *LNAw-SOw-SHWw*, AABW fills the lower half of the Atlantic basin as a result of the weaker and shallower NADW.

The northeastern Atlantic basin also features a middepth southward flow on the eastern side of the Mid-Atlantic Ridge (MAR) in *PI*, albeit much weaker (~3 Sv) than in the northwest Atlantic (Figure 4e), and which overlays a northward abyssal flow of southern-sourced waters. In contrast to the western Atlantic, as

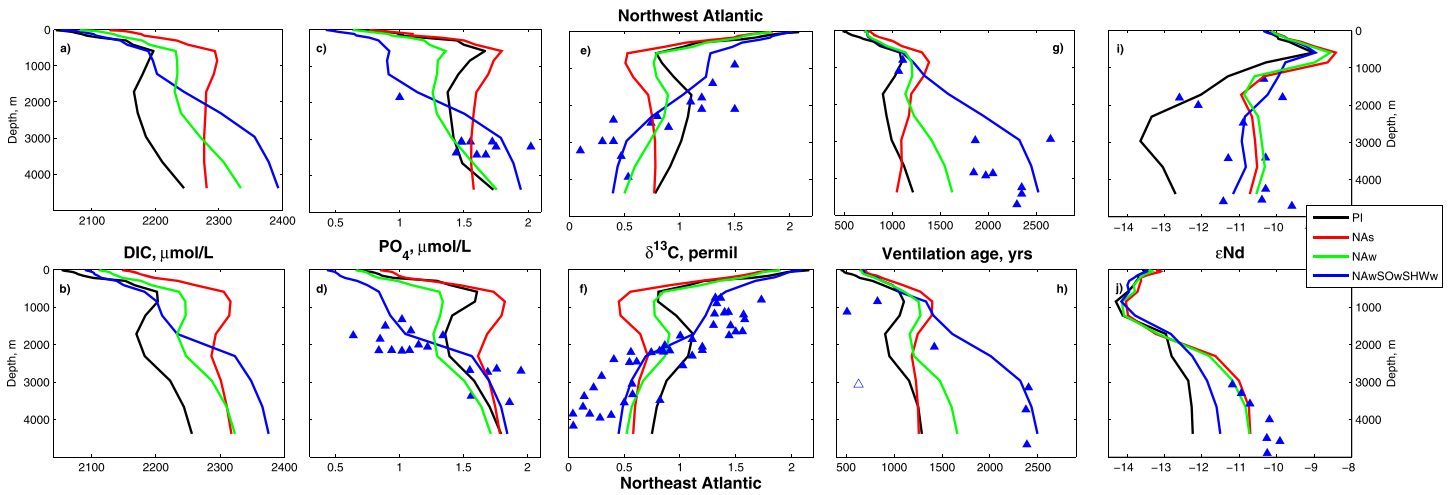


**Figure 3.** Tracers vertical profiles in the northwestern and northeastern Atlantic. Vertical profiles of (a, b) DIC ( $\mu\text{mol L}^{-1}$ ), (c, d)  $\text{PO}_4$  ( $\mu\text{mol L}^{-1}$ ), (e, f)  $\delta^{13}\text{C}$  (‰), (g, h) ventilation age (years) and (i, j)  $\epsilon\text{Nd}$  averaged over (top) the northwest Atlantic and (bottom) the northeast Atlantic for (black) the preindustrial control run, and the LGM states with strong NADW (red, LNAs), weak NADW (green, LNAw), and weak NADW and weak AABW (blue, LNAw-SOW-SHWw). The simulated variables are averaged over the areas that include proxy records:  $39\text{--}30^\circ\text{W}/41\text{--}65^\circ\text{N}$  and  $28\text{--}14^\circ\text{W}/42\text{--}62^\circ\text{N}$  for  $\text{PO}_4$ ,  $76\text{--}30^\circ\text{W}/28\text{--}56^\circ\text{N}$  and  $28\text{--}7^\circ\text{W}/27\text{--}61^\circ\text{N}$  for  $\delta^{13}\text{C}$ ,  $86\text{--}44^\circ\text{W}/0\text{--}44^\circ\text{N}$  and  $27\text{--}9^\circ\text{W}/5\text{--}38^\circ\text{N}$  for ventilation ages, and  $77\text{--}32^\circ\text{W}/12\text{--}41^\circ\text{N}$  and  $23\text{--}20^\circ\text{W}/18\text{--}25^\circ\text{N}$  for  $\epsilon\text{Nd}$ . For DIC the respective western and eastern basins are defined as follows:  $80\text{--}35^\circ\text{W}/30\text{--}60^\circ\text{N}$  and  $25^\circ\text{W}$  to  $0^\circ\text{E}/30\text{--}60^\circ\text{N}$ . The blue triangles indicate LGM, (c, d)  $\text{PO}_4$  estimates from Cd/Ca measurements (Marchitto, 2006) (Table S2), (e, f) benthic  $\delta^{13}\text{C}$  (Peterson et al., 2014) (Table S3), (g, h) ventilation age estimates from benthic foraminifera (filled triangles from Skinner et al., 2017, and empty triangle from Balmer & Sarinthein, 2018) (Table S4) and (i, j)  $\epsilon\text{Nd}$  data (Foster et al., 2007; Gutjahr et al., 2008; Roberts et al., 2010; Böhm et al., 2015; Howe et al., 2016; Land et al., 2016; Lippold et al., 2016; Howe et al., 2017) (Table S5).

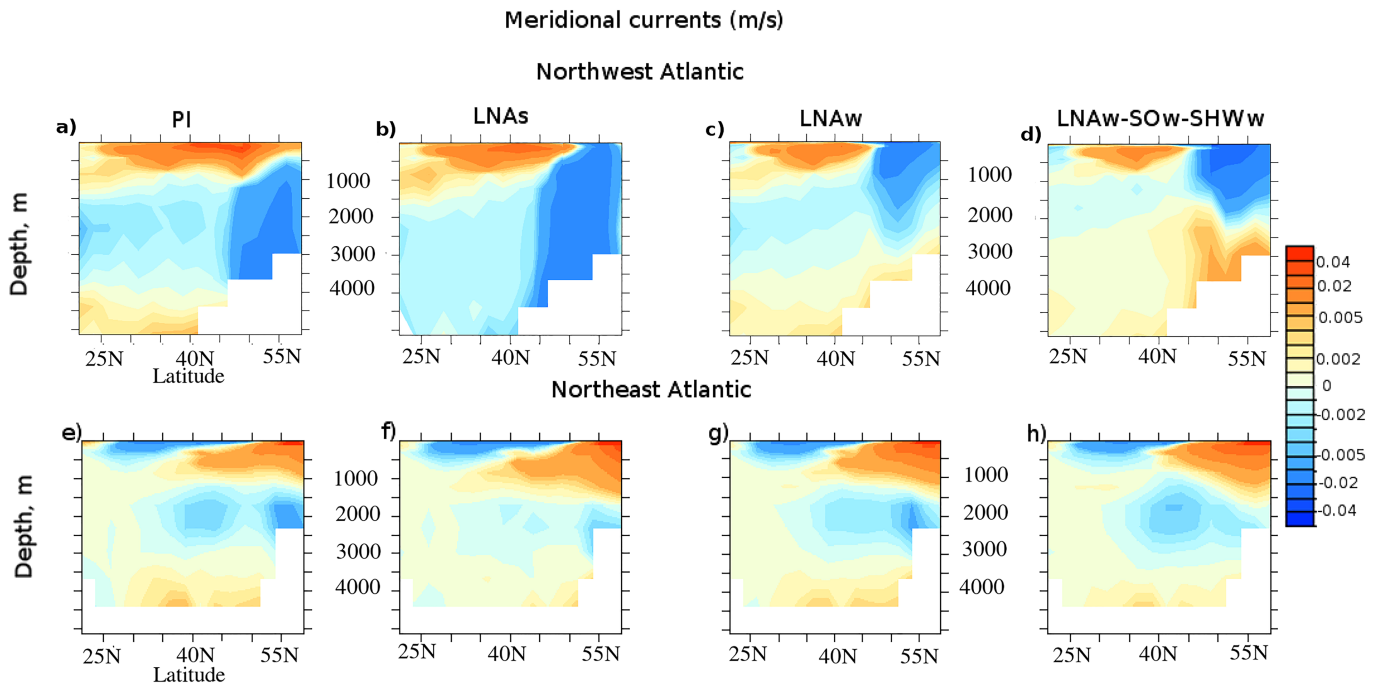


**Figure 4.** Northwestern (top row) and northeastern (bottom row) Atlantic meridional ocean currents (m/s) averaged over (top)  $80\text{--}38^\circ\text{W}$  until  $50^\circ\text{N}$  and  $43\text{--}38^\circ\text{W}$  north of that, (bottom)  $25^\circ\text{W}$  to  $0^\circ\text{E}$  for (a, e) the preindustrial control run (PI), and the LGM states with (b, f) a strong AMOC (LNAs), (c, g) a weak AMOC (LNAw), and (d, h) weak AMOC and weak AABW (LNAw-SOW-SHWw). Positive values indicate a northward flow.

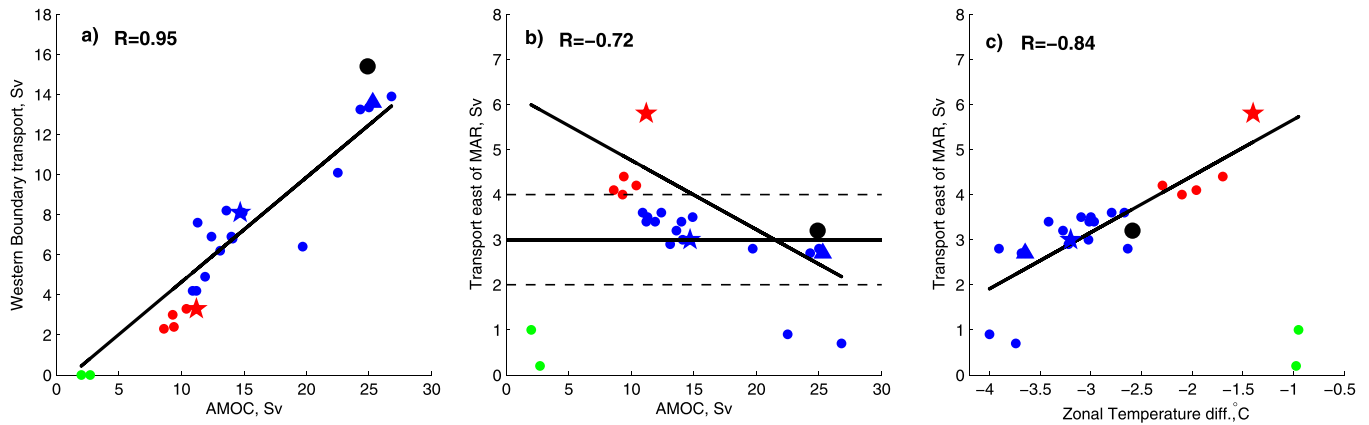


**Figure 5.** Relationship between AMOC and southward transport. (a) AMOC versus western boundary transport defined as the southward transport at  $30^{\circ}\text{N}/74\text{--}68^{\circ}\text{W}$ , and depths greater than 1,000 m (depth interval varies with the simulation to calculate only the southward flow, Table S1). (b) AMOC versus transport on the east side of the MAR defined as the southward transport at  $40^{\circ}\text{N}/22\text{--}16^{\circ}\text{W}$ , and depths greater than 1,000 m (depth interval varies with the simulation to calculate only the southward flow, Table S1); dashed lines represent  $\pm 1\sigma$ . (c) Zonal temperature gradient at  $\sim 50^{\circ}\text{N}$  and averaged over the upper 1,443 m depth ( $40\text{--}38^{\circ}\text{W}$  compared to  $24\text{--}20^{\circ}\text{W}$ ) versus transport on the east side of the MAR for a set of LGM experiments (section 2 and Table S1). The black dot is the preindustrial control run, the blue triangle is LNAs, the blue star is LNAw, and the red star is LNAw-SOw-SHWw. Red symbols indicate the simulations for which the transport on the east side of the MAR is significantly stronger ( $\geq 1\sigma$ ) than the preindustrial. Linear regressions (solid black lines) do not take into account the experiments with NADW off (represented by the green dots).

the AMOC weakens, the southward transport on the east side of the MAR intensifies (Figures 4g, 4h, and 5b,  $R = -0.72$ , and Figure 6). This southward transport is over  $1\sigma$  stronger than in *PI* (Figure 5, red symbols), when the AMOC is in an intermediate state (8.5 to 11 Sv), and the Nordic Sea convection site is at its southernmost location ( $\sim 65^{\circ}\text{N}$ , Figure 2d).

This intensification of middepth transport on the east side of the MAR is linked to a change in zonal density gradient and thus to changes in the potential vorticity field ( $q = -\frac{f}{\rho_0} \frac{\partial \rho}{\partial z}$ , with  $\rho$  the ocean density, and  $f$  the Coriolis parameter). Geostrophic flows do not easily flow across potential vorticity gradients. When the AMOC is strong, there is a strong zonal potential vorticity gradient at middepth north of  $45^{\circ}\text{N}$  that inhibits the zonal flow and directs the flow toward the DWBC (Figures 6a and 6b). This strong zonal potential vorticity gradient is in part due to zonal temperature differences (Figures 2 and 5c) arising from the North Atlantic Ocean circulation. Indeed, the NAC brings warm buoyant waters to the northeast Atlantic, reaching down to a depth of  $\sim 1,000$  m. By contrast, the northwest Atlantic is under the influence of the return flow of cold and fresh waters associated with the subpolar gyre, thus giving rise to a strong zonal temperature gradient (Figure 5c). As the AMOC weakens, so does the NAC, and thus the northeast Atlantic cools and lightens much more than the northwest Atlantic, reducing the zonal density gradient. The middepth zonal potential vorticity gradient north of  $45^{\circ}\text{N}$  decreases and is displaced westward (Figure 6c), thus allowing for a southward flow on both sides of the MAR. In LNAw-SOw-SHWw, the zonal potential vorticity gradient between  $45^{\circ}\text{N}$  and  $55^{\circ}\text{N}$  is weak, thus allowing the NADW to flow on the east side of the MAR (Figure 6d).

## 5. Comparison With Paleorecords and Implications

As NADW features low  $\text{PO}_4$ , and high  $\delta^{13}\text{C}$  compared to AABW, past AMOC changes can be inferred from geochemical analyses of marine sediment cores. The  $\text{PO}_4$  content will increase and  $\delta^{13}\text{C}$  will decrease as organic matter is remineralized and a water mass ages, but  $\delta^{13}\text{C}$  is also influenced by air-sea gas exchange. Since dissolved Cd distribution in the ocean is very similar to  $\text{PO}_4$ , past changes in seawater  $\text{PO}_4$  concentration can be estimated by measuring Cd/Ca in foraminifera shells (Marchitto, 2006).

In experiment LNAw-SOw-SHWw, as a result of the weaker and shallower NADW, AABW fills the lower half of the Atlantic basin despite AABW being weaker (Figure 4). This leads to a strong increase in vertical tracer gradients in the North Atlantic. Even though the AMOC is weaker, the  $\text{PO}_4$  concentration is low (below  $1.6 \mu\text{mol/L}$ ) and  $\delta^{13}\text{C}$  is high above  $\sim 2,000$  m depth, in agreement with LGM  $\delta^{13}\text{C}$  and Cd/Ca records (Marchitto, 2006; Peterson et al., 2014) (Figures 3c–3f, blue line and triangles). On the other hand, as suggested by proxy records, southern-sourced low  $\delta^{13}\text{C}$ /high  $\text{PO}_4$  waters reach both sides of the North Atlantic below  $\sim 2,500$  m depth (Figures 3c–3f, blue line and triangles).

Mid-depth potential vorticity  
anomalies and ocean currents

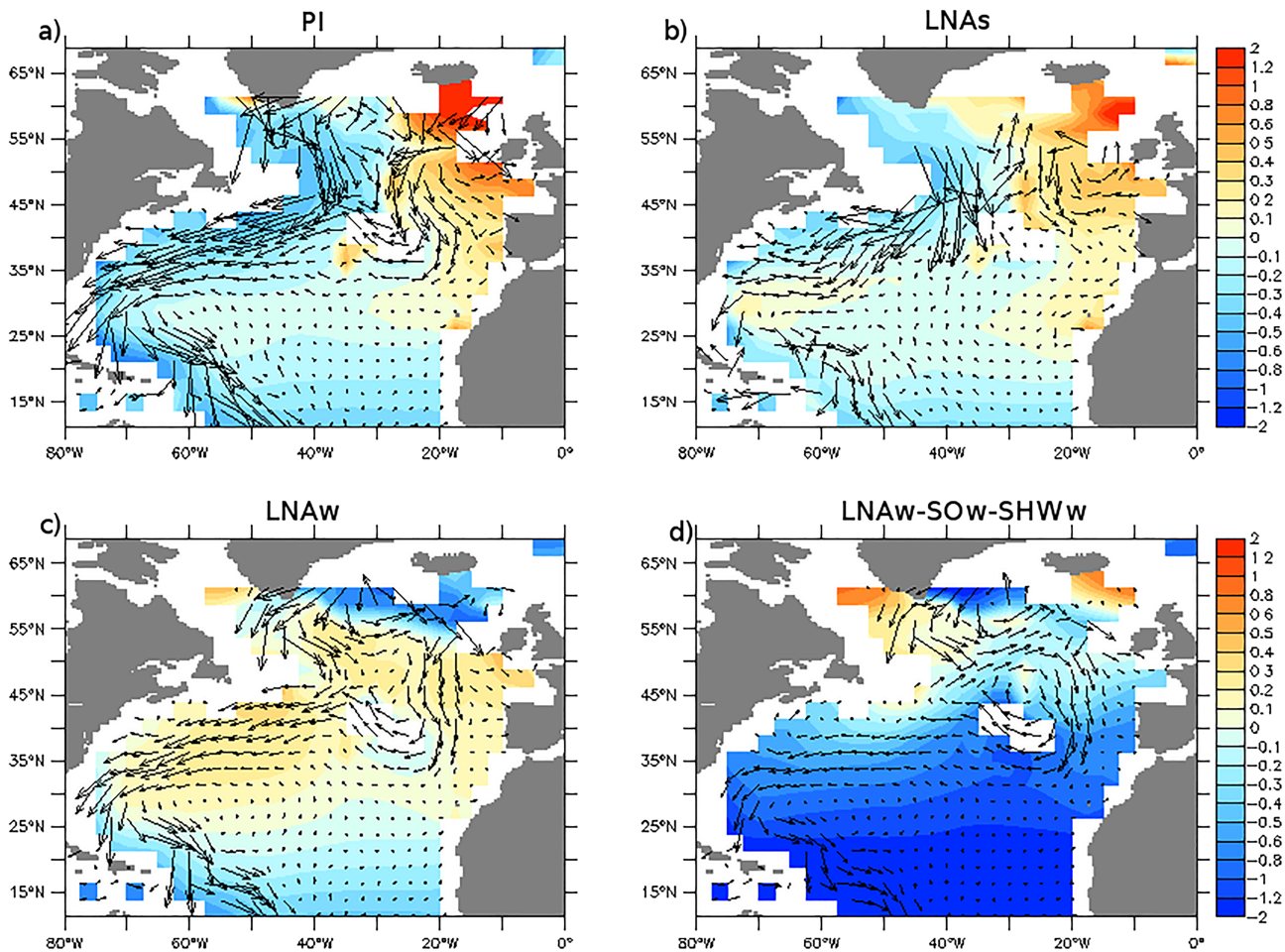


**Figure 6.** Mid-depth potential vorticity and ocean currents. Potential vorticity ( $q = -\frac{f}{\rho_0} \cdot \frac{\partial \rho}{\partial z}$ ) anomalies with respect to the northern North Atlantic (50–60°N/60–0°W,  $\text{m}^{-1} \cdot \text{s}^{-1}$ , shaded) at 1,443–2,622 m depth with currents (m/s) overlaid for (a) the preindustrial control run, and the LGM states with (b) strong NADW, (c) weak NADW, and (d) weak NADW and weak AABW.

To understand the processes leading to the positive  $\delta^{13}\text{C}$  anomaly simulated in the North Atlantic from the subsurface down to 1,500 m depth in *LNAw-SOW-SHWw*, the change in  $\delta^{13}\text{C}$  is decomposed into its biological ( $\delta^{13}\text{C}_{\text{BIO}}$ ) and thermodynamic ( $\delta^{13}\text{C}_{\text{TH}}$ ) components (Methods). As seen in Figure 7, the positive North Atlantic  $\delta^{13}\text{C}$  anomaly can be attributed at 70% to  $\delta^{13}\text{C}_{\text{BIO}}$  and at 30% to  $\delta^{13}\text{C}_{\text{TH}}$ . Even if a part of this  $\delta^{13}\text{C}_{\text{BIO}}$  could be due to the  $\sim 40\%$  lower export production in the North Atlantic, the changes in subsurface to middepth currents also significantly contribute. The weaker AMOC indeed leads to a reduction in the northward transport of intermediate-depth low latitude waters, with low  $\delta^{13}\text{C}$ /high  $\text{PO}_4$  concentration, to the northwest Atlantic (Figure 4). The change in  $\delta^{13}\text{C}_{\text{TH}}$  can be attributed to the strong surface cooling ( $-6.7^\circ\text{C}$ ), as well as to the southward shift of the convection site. Intermediate-depth North Atlantic  $\delta^{13}\text{C}$  anomalies are thus due to both a change in  $\delta^{13}\text{C}$  and  $\text{PO}_4$  NADW end-members, as well as to changes in oceanic circulation. It should however be noted that, as this decomposition method relies on calculating AOU from the saturated dissolved  $\text{O}_2$  concentration in the ocean,  $\delta^{13}\text{C}_{\text{BIO}}$  changes might be overestimated (Khaliwala et al., 2019).

Even if the simulated AMOC is weaker, the southward transport in the upper 1,500 m is still relatively strong and leads to ventilation ages within  $\sim 250$  years of *PI* (Figures 3g and 3h, blue line). As the deep North Atlantic is filled with southern-sourced waters, simulated ventilation ages below 3,000 m depth are  $\sim 1,500$  and 1,000 years higher in the northwest and northeast Atlantic, respectively, compared to *PI*. This is in good



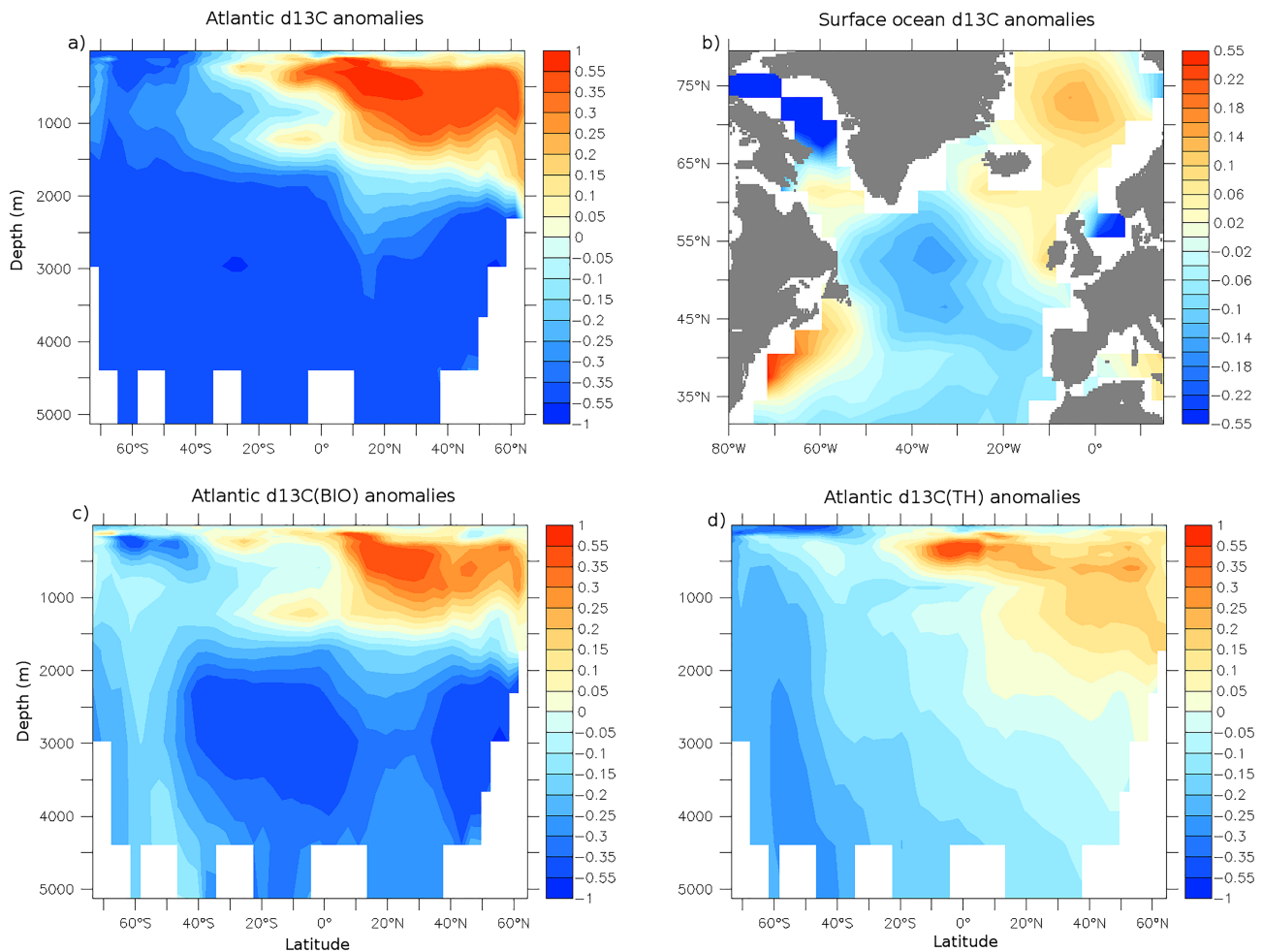


**Figure 7.** Attributing  $\delta^{13}\text{C}$  changes. (a)  $\delta^{13}\text{C}$  anomalies zonally averaged over the Atlantic; (b) surface  $\delta^{13}\text{C}$  anomalies; (c)  $\delta^{13}\text{C}_{\text{BIO}}$  and (d)  $\delta^{13}\text{C}_{\text{TH}}$  anomalies zonally averaged over the Atlantic (‰) for *LNAw-SOw-SHWw* compared to *PI*.

agreement with ventilation ages estimated from benthic foraminifera (Freeman et al., 2016; Skinner et al., 2017) (Figures 3g and 3h, blue filled triangles), even if the proxy records suggest that ventilation ages in the northwest Atlantic could be up to 400 years lower than in the northeast Atlantic between 3,000 and 4,000 m depth. The very low ventilation age estimated at 3,000 m depth on the Azores plateau (Figure 3h, empty blue triangle, Balmer & Sarinthein, 2018) is at odds with other North Atlantic measurements and cannot be reconciled with any of the simulations. The simulated transport in the deep northwest Atlantic could thus be a bit too weak in *LNAw-SOw-SHWw*, but paleoproxy records are consistent with a weaker circulation than the one simulated in *LNAw*.

The main difference in  $\epsilon\text{Nd}$  between the *PI* and all the LGM simulations is the lack of LSW, which induces a reduced zonal  $\epsilon\text{Nd}$  gradient in the North Atlantic at the LGM (Figures 3i and 3j). In the deep northeast Atlantic,  $\epsilon\text{Nd}$  decreases as AABW weakens (Figure 3j) because in the case of a “stagnant” ocean, boundary exchange with low- $\epsilon\text{Nd}$  boundaries such as the Gulf of Guinea, dominates the  $\epsilon\text{Nd}$  signature. This mismatch with proxy records could be due to a greater AABW  $\epsilon\text{Nd}$  end-member at the LGM, or an overestimated boundary exchange effect in the model.

This increase in North Atlantic vertical tracer gradient at the LGM is also seen in the simulated DIC profile, with relatively low DIC concentration at intermediate depth and high concentration below  $\sim 2,200$  m depth. Weak NADW and AABW thus allow carbon sequestration in the deep North Atlantic Ocean (Figures 3a and 3b), which would contribute to decreasing the atmospheric  $\text{CO}_2$  concentration at the LGM. As shown in Menviel et al. (2017), this weak oceanic circulation state allows for a 504 Gt C increase in deep ocean carbon.

## 6. Discussion and Conclusions

The LGM AMOC strength is modulated by several processes including the buoyancy of surface waters in the NADW formation region, itself being a function of the North Atlantic/Nordic Sea temperature and freshwater budget, the density contrast between NADW and AABW (Weber et al., 2007), North Atlantic windstress (Muglia & Schmittner, 2015; Sherriff-Tadano et al., 2018), and the closure of the Bering Strait (Hu et al., 2012). A stronger halocline in the Nordic Seas at the LGM would lead to sea ice advance, and a weakening of NADW formation (Oka et al., 2012). The simulations presented here suggest that sea ice advance at the LGM could have been associated with cessation of deep-ocean convection in the Labrador Sea, a southward shift of the convection site in the Norwegian Sea, and convection south of Iceland, thus leading to a weaker AMOC, consistent with benthic  $\delta^{18}\text{O}$  and  $\delta^{13}\text{C}$  records (Elmore et al., 2015; Meland et al., 2008; Millo et al., 2006). Furthermore, even in the most extreme scenario (*LNAw-SOw-SHWw*), the Norwegian Sea sea ice concentration is less than 50% for most of the year at  $\sim 66^\circ\text{N}$ , in agreement with paleoproxy records (de Vernal et al., 2006). In these simulations, the lack of a LSW signal is the dominant control on the Atlantic  $\epsilon\text{Nd}$  distribution, with NADW and AABW strength only playing relatively minor roles (Figures 3i and 3j). While the LGM simulation presented here agrees well with paleoproxy records of ocean surface conditions and North Atlantic ventilation, correctly simulating deep ocean convection is a challenge for ocean general circulation models (Heuzé, 2017). The location of convection and the respective strength of the convection sites should thus be further assessed in future studies.

For a range of deep ocean convection locations, the strength of the DWBC decreases with the AMOC (Figure 5a), thus supporting the hypothesis that changes in  $^{231}\text{Pa}/^{230}\text{Th}$  in the northwest Atlantic reflect AMOC changes (e.g., Gherardi et al., 2005; Henry et al., 2016; McManus et al., 2004). However, our simulations suggest that the middepth southward transport on the eastern side of the MAR will weaken only when NADW formation has almost ceased (Figure 5b). Therefore, ventilation records from the eastern side of the MAR will not directly reflect the AMOC strength.

The best fit with paleoproxy records is obtained for a LGM simulation with  $\sim 50\%$  reduced NADW and 40% weaker AABW (*LNAw-SOw-SHWw*), even though the oceanic circulation could potentially be a bit too weak in that scenario. Menviel et al. (2017) showed that another simulation with a similarly weak NADW, but AABW 11% weaker than PI (*LNAw-SOw*) could also provide a reasonable fit. However, the paleodata suggest strong vertical stratification in the North Atlantic at the LGM, which is best represented by simulation *LNAw-SOw-SHWw* (Figure 3, blue lines). Compared to PI, this simulation suggests a weaker flow on the western side and stronger flow on the eastern side of the MAR, which are both consistent with North Atlantic  $^{231}\text{Pa}/^{230}\text{Th}$  records (Ng et al., 2018).

Taking into account this east-west reorganization, we have shown that both northeastern and northwestern Atlantic proxy records are consistent with a weaker AMOC at the LGM. In addition, southern-sourced waters can fill the North Atlantic below  $\sim 2,500$  m depth despite the AABW transport being reduced.

Compared to an LGM state with a strong AMOC, a LGM simulation with weak AMOC leads to an increase in deep (below 2,600 m depth) ocean carbon content of 216 Gt C, while a LGM simulation with weak NADW and AABW leads to a 504 Gt C increase (Menviel et al., 2017). A globally weaker ocean circulation in the Atlantic at the LGM, as consistent with proxy records, would thus contribute to lowering atmospheric  $\text{CO}_2$  by increasing the oceanic carbon content. However, future studies will need to detail the physical processes leading to such a weak oceanic circulation at the LGM.

### Data Availability Statement

The paleoproxy data described in this study and the data from Figure 3 are available in the supporting information. Results of the modeling experiments are available through UNSW ResData ([http://handle.unsw.edu.au/1959.4/resource/collection/resdatac\\_862/1](http://handle.unsw.edu.au/1959.4/resource/collection/resdatac_862/1), under the DOI: <https://doi.org/10.26190/5e1ce1e12f00f>).

### References

- Abe-Ouchi, A., Saito, F., Kageyama, M., Braconnot, P., Harrison, S. P., Lambeck, K., et al. (2015). Ice-sheet configuration in the CMIP5/PMIP3 Last Glacial Maximum experiments. *Geoscientific Model Development*, 8(11), 3621–3637. <https://doi.org/10.5194/gmd-8-3621-2015>

### Acknowledgments

This project was supported by the Australian Research Council. L. C. M., L. M., P. S., and J. Y. acknowledge funding from the Australian Research Council Grants DE150100107, DP180100048, DE150100223, FT140100993, FT180100606, and DP140101393. L. C. S. acknowledges support from NERC Grant NE/L006421/1. This work also benefited from discussions and interactions made possible by the INQUA “IPODS” (Investigating Past Ocean Dynamics) focus group. LOVECLIM experiments were performed on a computational cluster owned by the Faculty of Science of the University of New South Wales, Sydney, Australia.

- Abe-Ouchi, A., Segawa, T., & Saito, F. (2007). Climatic conditions for modelling the Northern Hemisphere ice sheets throughout the Ice Age cycle. *Climate of the Past*, 3, 423–438.
- Balmer, S., & Sarnthein, M. (2018). Glacial-to-deglacial changes in North Atlantic meltwater advection and deep-water formation—Centennial-to-millennial-scale  $^{14}\text{C}$  records from the Azores plateau. *Geochimica et Cosmochimica Acta*, 236, 399–415. <https://doi.org/10.1016/j.gca.2018.03.001>
- Bentley, M. J., Cofaigh, C., Anderson, J. B., Conway, H., Davies, B., Graham, A. G., et al. (2014). A community-based geological reconstruction of Antarctic Ice Sheet deglaciation since the Last Glacial Maximum. *Quaternary Science Reviews*, 100, 1–9. <https://doi.org/10.1016/j.quascirev.2014.06.025>
- Berger, A. (1978). Long term variations of daily insolation and Quaternary climate change. *Journal of the Atmospheric Sciences*, 35, 2362–2367.
- Böhm, E., Lippold, J., Gutjahr, M., Frank, M., Blaser, P., Antz, B., et al. (2015). Strong and deep Atlantic meridional overturning circulation during the last glacial cycle. *Nature*, 517, 73–76.
- Bradt Miller, L., McManus, J., & Robinson, L. (2014).  $^{231}\text{Pa}/^{230}\text{Th}$  evidence for a weakened but persistent Atlantic meridional overturning circulation during Heinrich Stadial 1. *Nature Communications*, 5, 5817.
- Bullister, J. L., Rhein, M., & Mauritzen, C. (2013). Chapter 10—Deepwater formation. In G. Siedler, S. M. Griffies, J. Gould, & J. A. Church (Eds.), *Ocean circulation and climate* (Vol. 103, pp. 227–253). Academic Press. <https://doi.org/10.1016/B978-0-12-391851-2.00010-6>
- Curry, W., & Oppo, D. (2005). Glacial water mass geometry and the distribution of  $\delta^{13}\text{C}$  of  $\Sigma\text{CO}_2$  in the western Atlantic Ocean. *Paleoceanography*, 20, PA1017. <https://doi.org/10.1029/2004PA001021>
- De Boer, A. M., & Hogg, A. M. (2014). Control of the glacial carbon budget by topographically induced mixing. *Geophysical Research Letters*, 41, 4277–4284. <https://doi.org/10.1002/2014GL059963>
- de Vernal, A., Rosell-Melé, A., Kucera, M., Hillaire-Marcel, C., Eynaud, F., Weinelt, M., et al. (2006). Comparing proxies for the reconstruction of LGM sea-surface conditions in the northern North Atlantic. *Quaternary Science Reviews*, 25(21), 2820–2834. <https://doi.org/10.1016/j.quascirev.2006.06.006>
- Elmore, A., Wright, J., & Chalk, T. (2015). Precession-driven changes in Iceland-Scotland Overflow Water penetration and bottom water circulation on Gardar Drift since ~200 ka. *Palaeogeography, Palaeoclimatology, Palaeoecology*, 440, 551–563. <https://doi.org/10.1016/j.palaeo.2015.09.042>
- Foster, G., Vance, D., & Prytulak, J. (2007). No change in the neodymium isotope composition of deep water exported from the North Atlantic on glacial-interglacial time scales. *Geology*, 35, 37–40.
- Freeman, E., Skinner, L., Waelbroeck, C., & Hodell, D. (2016). Radiocarbon evidence for enhanced respired carbon storage in the Atlantic at the Last Glacial Maximum. *Nature Communications*, 7, 11998. <https://doi.org/10.1038/ncomms11998>
- Friedrich, T., Timmermann, A., Stichel, T., & Pahnke, K. (2014). Ocean circulation reconstructions from  $\epsilon_{\text{Nd}}$ : A model-based feasibility study. *Paleoceanography*, 29, 1003–1023. <https://doi.org/10.1002/2014PA002658>
- Gherardi, J., Labeyrie, L., McManus, J., Francois, R., Skinner, L., & Cortijo, E. (2005). Evidence from the northeastern Atlantic basin for variability in the rate of the meridional overturning circulation through the last deglaciation. *Earth and Planetary Science Letters*, 240, 710–723.
- Gosse, H., Brovkin, V., Fichefet, T., Jongma, J., Huybrechts, P., Mouchet, A., et al. (2010). Description of the Earth system model of intermediate complexity LOVECLIM version 1.2. *Geoscientific Model Development*, 3, 603–633.
- Gutjahr, M., Frank, M., Stirling, C., Keigwin, L., & Halliday, A. (2008). Tracing the Nd isotope evolution of North Atlantic Deep and Intermediate Waters in the western North Atlantic since the Last Glacial Maximum from Blake Ridge sediments. *Earth and Planetary Science Letters*, 266, 61–77.
- Henry, L., McManus, J., Curry, B., Roberts, N., Piotrowski, A., & Keigwin, L. (2016). North Atlantic Ocean circulation and abrupt climate change during the last glaciation. *Science*, 353, 470–474. <https://doi.org/10.1126/science.aaf5529>
- Hesse, T., Butzin, M., Bickert, T., & Lohmann, G. (2011). A model-data comparison of  $\delta^{13}\text{C}$  in the glacial Atlantic Ocean. *Paleoceanography*, 26, PA3220. <https://doi.org/10.1029/2010PA002085>
- Heuzé, C. (2017). North Atlantic deep water formation and AMOC in CMIP5 models. *Ocean Science*, 13(4), 609–622. <https://doi.org/10.5194/os-13-609-2017>
- Howe, J. N., Piotrowski, A. M., Hu, R., & Bory, A. (2017). Reconstruction of east-west deep water exchange in the low latitude Atlantic Ocean over the past 25,000 years. *Earth and Planetary Science Letters*, 458, 327–336. <https://doi.org/10.1016/j.epsl.2016.10.048>
- Howe, J., Piotrowski, A., Noble, T., Mulitza, S., Chiessi, C., & Bayon, G. (2016). North Atlantic Deep Water production during the Last Glacial Maximum. *Nature Communications*, 7, 11765. <https://doi.org/10.1038/ncomms11765>
- Hu, A., Meehl, G., Han, W., Timmermann, A., Otto-Bliesner, B., Liu, Z., et al. (2012). Role of the Bering Strait on the hysteresis of the ocean conveyor belt circulation and glacial climate stability. *Proceedings of the National Academy of Sciences of the USA*, 107, 6417–6422. <https://doi.org/10.1073/pnas.1116014109>
- Khatiwala, S., Schmittner, A., & Muglia, J. (2019). Air-sea disequilibrium enhances ocean carbon storage during glacial periods. *Science Advances*, 5(6), eaaw4981. <https://doi.org/10.1126/sciadv.aaw4981>
- Krebs, U., & Timmermann, A. (2007). Tropical air-sea interactions accelerate the recovery of the Atlantic Meridional Overturning Circulation after a major shutdown. *Journal of Climate*, 20, 4940–4956.
- Kurahashi-Nakamura, T., Paul, A., & Losch, M. (2017). Dynamical reconstruction of the global ocean state during the Last Glacial Maximum. *Paleoceanography*, 32(4), 326–350. <https://doi.org/10.1002/2016PA003001>
- Lambeck, K., Rouby, H., Purcell, A., Sun, Y., & Sambridge, M. (2014). Sea level and global ice volumes from the Last Glacial Maximum to the Holocene. *Proceedings of the National Academy of Sciences*, 111(43), 15,296–15,303. <https://doi.org/10.1073/pnas.1411762111>
- Land, D., Bailey, I., Wilson, P., Chalk, T., Foster, G., & Gutjahr, M. (2016). Incursions of southern-sourced water into the deep North Atlantic during late Pliocene glacial intensification. *Nature Geoscience*, 9, 375–379.
- Lippold, J., Gutjahr, M., Blaser, P., Christner, E., de Carvalho Ferreira, M., Mulitza, S., et al. (2016). Deep water provenance and dynamics of the (de)glacial Atlantic meridional overturning circulation. *Earth and Planetary Science Letters*, 445, 68–78. <https://doi.org/10.1016/j.epsl.2016.04.013>
- Lippold, J., Luo, Y., Francois, R., Allen, S., Gherardi, J., Pichat, S., et al. (2012). Strength and geometry of the glacial Atlantic Meridional Overturning Circulation. *Nature Geoscience*, 5, 813–816.
- Lozier, M. S., Li, F., Bacon, S., Bahr, F., Bower, A. S., Cunningham, S. A., et al. (2019). A sea change in our view of overturning in the subtropical North Atlantic. *Science*, 363(6426), 516–521. <https://doi.org/10.1126/science.aau6592>
- Marchitto, T. (2006). Deep water mass geometry in the glacial Atlantic Ocean: A review of constraints from the paleonutrient proxy Cd/Ca. *Geochemistry Geophysics Geosystems*, 7, Q12003. <https://doi.org/10.1029/2006GC001323>

- Marcott, S., Clark, P., Padman, L., Klinkhammer, G., Springer, S., Liu, Z., et al. (2011). Ice-shelf collapse from subsurface warming as trigger for Heinrich events. *Proceedings of the National Academy of Sciences*, *108*, 13,415–13,419. <https://doi.org/10.1073/pnas.1104772108>
- McManus, J. F., Francois, R., Gherardi, J. M., Keigwin, L. D., & Brown-Leger, S. (2004). Collapse and rapid resumption of Atlantic meridional circulation linked to deglacial climate changes. *Nature*, *428*, 834–837.
- Meland, M., Dokken, T., Jansen, E., & Hevrøy, K. (2008). Water mass properties and exchange between the Nordic seas and the northern North Atlantic during the period 23–6 ka: Benthic oxygen isotopic evidence. *Paleoceanography*, *23*, PA1210. <https://doi.org/10.1029/2007PA001416>
- Menviel, L., Mouchet, A., Meissner, K., Joos, F., & England, M. (2015). Impact of oceanic circulation changes on atmospheric  $\delta^{13}\text{C}_{\text{O}_2}$ . *Global Biogeochemical Cycles*, *29*, 1944–1961. <https://doi.org/10.1002/2015GB005207>
- Menviel, L., Yu, J., Joos, F., Mouchet, A., Meissner, K., & England, M. (2017). Poorly ventilated deep ocean at the Last Glacial Maximum inferred from carbon isotopes: A data-model comparison study. *Paleoceanography*, *32*, 2–17. <https://doi.org/10.1002/2016PA003024>
- Millo, C., Sarnthein, M., Voelker, A., & Erlenkeuser, H. (2006). Variability of the Denmark Strait overflow during the Last Glacial Maximum. *Boreas*, *35*(1), 50–60. <https://doi.org/10.1111/j.1502-3885.2006.tb01112.x>
- Muglia, J., & Schmittner, A. (2015). Glacial Atlantic overturning increased by wind stress in climate models. *Geophysical Research Letters*, *42*, 9862–9868. <https://doi.org/10.1002/2015GL064583>
- Muglia, J., Skinner, L. C., & Schmittner, A. (2018). Weak overturning circulation and high Southern Ocean nutrient utilization maximized glacial ocean carbon. *Earth and Planetary Science Letters*, *496*, 47–56. <https://doi.org/10.1016/j.epsl.2018.05.038>
- Ng, H., Robinson, L., McManus, J., Mohamed, K., Jacobel, A., Ivanovic, R., et al. (2018). Coherent deglacial changes in deep Atlantic Ocean circulation. *Nature Communications*, *9*, 2947. <https://doi.org/10.1038/s41467-018-05312-3>
- Oka, A., Hasumi, H., & Abe-Ouchi, A. (2012). The thermal threshold of the Atlantic meridional overturning circulation and its control by wind stress forcing during glacial climate. *Geophysical Research Letters*, *39*, L09709. <https://doi.org/10.1029/2012GL051421>
- Peterson, C., Lisiecki, L., & Stern, J. (2014). Deglacial whole-ocean  $\delta^{13}\text{C}$  change estimated from 480 benthic foraminiferal records. *Paleoceanography*, *29*, 549–563. <https://doi.org/10.1002/2013PA002552>
- Roberts, N., Piotrowski, A., McManus, J., & Keigwin, L. (2010). Synchronous deglacial overturning and water mass source changes. *Science*, *327*, 75–78.
- Sherriff-Tadano, S., Abe-Ouchi, A., Yoshimori, M., Oka, A., & Chan, W. L. (2018). Influence of glacial ice sheets on the Atlantic meridional overturning circulation through surface wind change. *Climate Dynamics*, *50*(7), 2881–2903. <https://doi.org/10.1007/s00382-017-3780-0>
- Skinner, L., Primeau, F., Freeman, E., de la Fuente, M., Goodwin, P., Gottschalk, J., et al. (2017). Radiocarbon constraints on the glacial ocean circulation and its impact on atmospheric  $\text{CO}_2$ . *Nature Communications*, *8*, 16010. <https://doi.org/10.1038/ncomms16010>
- Tachikawa, K., Arsouze, T., Bayon, G., Bory, A., Colin, C., Dutay, J. C., et al. (2017). The large-scale evolution of neodymium isotopic composition in the global modern and Holocene ocean revealed from seawater and archive data. *Chemical Geology*, *457*, 131–148. <https://doi.org/10.1016/j.chemgeo.2017.03.018>
- Tagliabue, A., Bopp, L., Roche, D., Bouttes, N., Dutay, J. C., Alkama, R., et al. (2009). Quantifying the roles of ocean circulation and biogeochemistry in governing ocean carbon-13 and atmospheric carbon dioxide at the Last Glacial Maximum. *Climate of the Past*, *5*, 695–706.
- Talley, L. D., Pickard, G. L., Emery, W. J., & Swift, J. H. (2011). Chapter S9—Atlantic Ocean: Supplementary materials, (6th ed.), *Descriptive physical oceanography (sixth edition)* (pp. 1–43). Boston: Academic Press. <https://doi.org/10.1016/B978-0-7506-4552-2.10021-6>
- Tarasov, L., Dyke, A. S., Neal, R. M., & Peltier, W. R. (2012). A data-calibrated distribution of deglacial chronologies for the North American ice complex from glaciological modeling. *Earth and Planetary Science Letters*, *315–316*, 30–40.
- Toggweiler, J., Russell, J., & Carson, S. (2006). Midlatitude westerlies, atmospheric  $\text{CO}_2$ , and climate change during ice ages. *Paleoceanography*, *21*, PA2005. <https://doi.org/10.1029/2005PA001154>
- Weber, S., Drijfhout, S., Abe-Ouchi, A., Crucifix, M., Eby, M., Ganopolski, A., et al. (2007). The modern and glacial overturning circulation in the Atlantic ocean in PMIP coupled model simulations. *Climate of the Past*, *3*, 51–64.
- Yang, D., Myers, P. G., & Bush, A. B. G. (2006). Sensitivity of the subpolar North Atlantic to Last Glacial Maximum surface forcing and sea ice distribution in an eddy-permitting regional ocean model. *Paleoceanography*, *21*, PA2013. <https://doi.org/10.1029/2005PA001209>
- Yu, J., Elderfield, H., & Piotrowski, A. (2008). Seawater carbonate ion- $\delta^{13}\text{C}$  systematics and application to glacial-interglacial North Atlantic ocean circulation. *Earth and Planetary Science Letters*, *271*, 209–220.